We are IntechOpen, the world's leading publisher of Open Access books Built by scientists, for scientists

6,900
Open access books available

185,000
International authors and editors

200M
Downloads

Our authors are among the

154
Countries delivered to

TOP 1%
most cited scientists

12.2%
Contributors from top 500 universities



WEB OF SCIENCE™

Selection of our books indexed in the Book Citation Index in Web of Science™ Core Collection (BKCI)

Interested in publishing with us?
Contact book.department@intechopen.com

Numbers displayed above are based on latest data collected.
For more information visit www.intechopen.com



15

Computation of Flows in Steam Generators

Dr Jonas Bredberg
Epsilon UC Väst
Sweden

1. Introduction

This chapter will be devoted to explain the foundations of Computational Fluid Dynamics (CFD), and its possible application to simulate flow conditions in steam generators of pressurized water reactors (PWR). Besides steam generator application simulations, test cases will be included to show the ability of CFD to faithfully reproduce some fundamental heat and flow phenomena

The common design of a PWR steam generator is a vertical standing U-tube heat exchanger divided into a number of stages with separator plates (baffles) in between, as seen in Fig. 1. Several thousands of tubes is not unusual which consequently puts significant strain on computational resources if all details are to be resolved. The multitude of tubes and several stages however facilitates the possibility to study characteristic sections of the heat exchanger with reasonable confidence on flow conditions (i.e. boundary condition) and with a required accuracy.

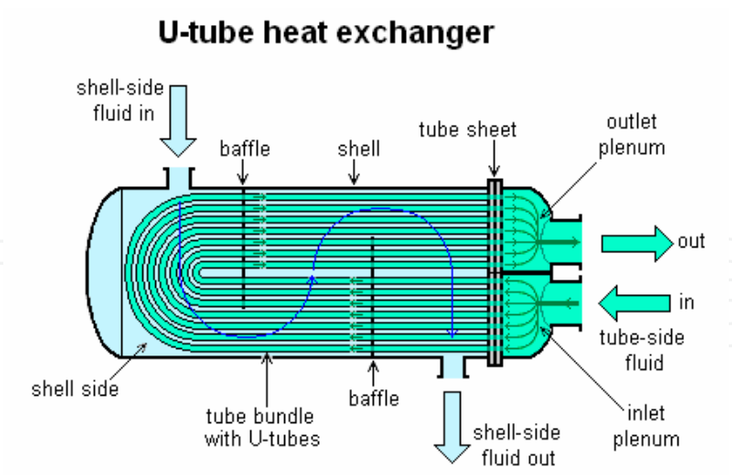


Fig. 1. Typical lay-out of U-tube heat exchanger, similar in concept to the design of steam generators as found in a PWR

The steam generator is divided into i) a primary side, where hot pressurized water from the reactor core flows, and ii) a secondary side, where relatively cold water is heated and evaporated to generate steam for the turbines. The division of the PWR into a primary- and secondary side (as opposed to a BWR, Boiling Water Reactor) is of major advantage for

safety reasons as the contaminated water on the primary side can be enclosed in a smaller and sealed off compartment.

In regards to simulating and predicting the conditions in the primary side, there is only minor obstacles, since the case of a single-phase fluid (superheated water), flowing in a pipe with external cooling (heating and boiling of the water on the secondary side) is a well defined and abundantly studied system. Pipe-flow is one of the cornerstones for developing numerics and models for CFD codes, and can now be considered to be mastered to a high degree of accuracy. The only part that may need some attention is the plenum with its inlet/outlet and the bend section with local effects from separation and secondary flow. The conditions within the pipe could even with little hesitation be estimated from well known correlation for internal pipe flow.

The flow on the secondary side need however to be more carefully treated, particularly as it includes two-phase boiling. To simulate this flow the CFD models and numerics need to capture:

- Wall interaction and shearing
- Streamline curvature
- Flow separation and re-attachment
- Heat transfer
- Boiling
- Buoyancy

In single-phase regimes the above criteria mainly put demands on turbulence modelling, particularly in the case of accurate heat transfer predictions, which obviously is of major importance in heat exchanger performance. Fortunately, turbulence theory and modelling has advanced significantly the last couples of decades and has now reached a mature level of predictability that, through proper choice can predict pressure drop and heat transfer within measurement accuracy. In the two-phase regime, the choice of multi-phase models is obvious of great importance, but also specific boiling models and bubble-dynamic models. CFD programs has not yet progress to a similar level of maturity for two-phase flow, although through a high-degree of mesh refinement and employing direct simulations (DNS/LES) all phenomena found in nature can be resolved, albeit at an extreme expense of computational resources. One is thus normally restricted to an engineering or global model for two-phase problems which are designed to capture the main characteristics of the flow, rather than all details. In forthcoming discussions, such models and examples of using them will not be included.

The following two sections are primarily based on the work performed by the author forming a basis for his Ph.D. (Bredberg, 2002). This introductory section and last sections are mainly based on the work within the ARTIST group (Güntay, et. al., 2004), (Berg et. al., 2008a) and (Berg et. al., 2008b)

2. Foundations of CFD

2.1 Governing equations

The equations that govern fluid motion and heat transfer are the continuity, momentum and energy equations. These equations, were independently derived by Navier (in 1822) and Stokes (in 1845) and are commonly referred to as the Navier-Stokes equations, albeit it was only the momentum equation that both Navier and Stokes were referring to. These

equations can be formulated in either a conservative form, or in a non-conservative, density normalized form.

Continuity

The continuity equation states the conservation of mass, which for all but nuclear-reaction environments is valid. Its conservative form is:

$$\frac{\partial \rho}{\partial t} + \frac{\partial \rho U_i}{\partial x_i} = 0 \tag{1}$$

Momentum

The momentum equation describes a force-balance, which – from Newtons second law - states that the mass times the acceleration is equal to imposed forces. The forces are divided into body force F_i, eg. the gravitational force, and surface forces, T_{ij}. The surfaces forces are normally written as a combination of pressure (normal stress) and viscous stresses (shear) as:

$$T_{ij} = -P\delta_{ij} + \tau_{ij} \tag{2}$$

Assuming a Newtonian incompressible fluid the momentum equations become:

$$\frac{\partial \rho U_i}{\partial t} + \frac{\partial \rho U_i U_j}{\partial x_i} = \rho g_i + F_i - \frac{\partial P}{\partial x_i} + \frac{\partial}{\partial x_j}(2\mu S_{ij}) \tag{3}$$

where F_i is any additional body-forces that can effect the fluid motion such as rotation, a magnetic- or electric-field etc.

Energy

The first law of thermodynamics states that the exchange of energy in a system is the result of applied work and heat transfer through that region. In its most complete formulation the energy equations is given as (Panton, 1995):

$$\frac{\partial \rho E_0}{\partial t} + \frac{\partial \rho U_i E_0}{\partial x_i} = \rho U_i F_i - \frac{\partial q_i}{\partial x_i} + \frac{\partial}{\partial x_j}(U_i T_{ij}) \tag{4}$$

where T_{ij} is the surface forces similar to the viscous and pressure terms in the momentum equations. E_0 is the total internal energy, including the kinetic energy. The energy equation as displayed above is however seldom used and instead the simplified temperature equation is applied:

$$\frac{\partial \rho C_p T}{\partial t} + \frac{\partial \rho C_p T U_i}{\partial x_i} = \frac{\partial}{\partial x_j}\left(\frac{\mu C_p}{Pr}\frac{\partial T}{\partial x_i}\right) \tag{5}$$

2.2 Flow models

The Navier-Stokes equations are composed of non-linear partial differential equations with an intricate complex dependency within the equation system. Partial differential equations are apart from some specific cases, not solvable using known mathematical tools hence the NS-equations impose a severe obstacle to the physical world. There are only a very small

number of flows that entitle one to simplify the governing equations in such a way that it is possible to achieve an analytical solution. Consequently for most cases, one is referred to numerically solve the Navier-Stokes equations. The highest level of fidelity is given by Direct Numerical Simulations (DNS) and Large Eddy Simulations (LES). Numerical simulations performed using Reynolds Averaged Navier Stokes (RANS) solvers are apart from numerical approximations also affected by physical approximations - in the models for the turbulence field.

Direct Simulation (DNS/LES)

Direct Numerical Simulations (DNS) and Large Eddy Simulations (LES) both solve the equations in the four-dimensional room, time and space. The additional modelling in LES as compared to DNS is the introduction of a sub-grid scale (SGS) model (Smagorinsky, 1963) which legitimacy is based on the assumption of isotropocy of the smallest scales. For a given cut-off wave-length, normally related to the grid-size, LES don't resolve the smallest length-scales but rather approximate them using the SGS-model. DNS are much appreciated as they are considered equally, or even more accurate than experiments. The numerical model enable unphysical although theoretical interesting flows to be simulated, with a degree of control unachievable in a laboratory. The numerical accuracy in DNS are usually much higher than the uncertainty in any measuring tool. A major drawback is however that the simulations are computational expansive and can only be performed on a limited numberof flows, all with relatively low Reynolds numbers.

Reynolds Averaged Navier-Stokes (RANS)

Nearly all numerical simulations are performed using various RANS-models, as a consequence of the excessive computational resources needed for a DNS. Reynolds (Reynolds, 1895) proposed that the quantities in the Navier-Stokes-equation could be divided into a mean and a fluctuating part:

$$\phi = \bar{\phi} + \phi' \tag{6}$$

where the mean part is the time-average of a parameter over a certain time. The averaging time needs to be longer than the small turbulent fluctuation, however shorter than any mean flow oscillating period. If Reynolds decomposition is applied to the Navier-Stokes equation the result is an equivalent set of equations, the Reynolds Averaged Navier-Stokes equations. For a though and comprehensive analysis of the averaging see e.g. Hinze (Hinze, 1975). The difference between the former and the original are that the RANS equations not only involves time-averaged quantities but also produces an additional term, the Reynolds stresses:

$$\tau_{ij} = \overline{u_i u_j} \tag{7}$$

which are unknown and need to be modelled using a turbulence model. This is referred to as the closure problem with Reynolds averaging.

There are two distinct approaches to model the Reynolds stresses, either the eddy-viscosity models (EVM), or the Reynolds stress models (RSM). In the latter the actual stresses are solved, while in the former the Boussinesq hypothesis (Boussinesq, 1877) is employed to estimate τ_{ij}. In its simplest form, the eddy-viscosity μ_t is computed based on some geometrical/flow conditions. In the commonly employed two-equation turbulence models, the eddy-viscosity is computed using two turbulent quantities, the turbulent kinetic energy,

k, and a length-scale determining quantity (ε, ω, τ or l). In a strive to enhance the performance of the two-equation EVMs researchers have proposed non-linear EVMs, which include, apart from the Boussinesq hypothesis, additional terms to determine the eddy-viscosity.
The ASM and EARSM (or EASM) are different in that they compute the Reynolds stresses using algebraic equations. In ASM the convective and diffusion terms in the Reynolds stress transport equations are approximated using anisotropized versions of the same terms in the turbulent kinetic energy. The ASM thus only need to solve two transport equations, that for k and an additional secondary turbulence quantity. The Reynolds stresses could then be estimated using the constructed algebraic relations. This modelling approach is however prone to numerical instable solution and are seldom used. It is possible, through the use of the Cayley-Hamilton theorem to derive the complete tensorial relation for the Reynolds stresses, expression in the strain-rate tensor, S_{ij} and the rotation tensor, Ω_{ij}. The complete set involves ten terms with their respective coefficients (Pope, 1975). Using these expressions the Reynolds stresses can, in a second moment closure sense, be exactly computed. EARSMs are thus theoretically more correct than non-linear EVMs, although the final expressions are often confusingly similar. They differ in the approach used for the coefficients in the tensor groups, which in EARSMs, at least for 2D-flows, can be based on derived analytic expressions (Wallin & Johansson, 2000).

2.3 Turbulence models

Reynolds Stress Models (RSM)
The Reynolds Stress Models (RSM) (Launder, 1989) solves the Reynolds stresses;

$$\tau_{ij} = \overline{u_i u_j} \tag{8}$$

using individual transport equations. RSM based RANS-codes thus include, apart from three momentum equation, six stress equation, and an additional length-scale determining equation. The transport equations for the Reynolds stresses are:

$$\frac{D\tau_{ij}}{Dt} = P_{ij} + G_{ij} + \Pi_{ij} - \varepsilon_{ij} + \frac{\partial D_{ij}^{T}}{\partial x_k} + \frac{\partial D_{ij}^{v}}{\partial x_k} \tag{9}$$

where P_{ij} is the shear production term, Π_{ij} the pressure-strain term, ε_{ij} the dissipation term, D^{T}_{ij} turbulent transport (diffusion) term, D^{v}_{ij} and the viscous diffusion term. For a complete derivation and expansion see e.g. Bredberg (Bredberg, 1999). The production terms, and the viscous diffusion term are exact in the context of a Reynolds Stress Model. The other terms need however be modelled. The exact formulation of the production terms is a fundamental advantage of the RSMs compared to the EVMs, e.g. for rotating flow.

Eddy-Viscosity Models (EVM)

The eddy-viscosity concept is based on similar reasoning that turbulence is a physical concept connected to the viscosity. It can be argued that similar to viscosity, turbulence affects the dissipation, diffusion and mixing processes. Thus it is reasonable to model the Reynolds stresses in a fashion closely related to the viscous term. The Reynolds stress term produced by the Reynolds-averaging is:

$$D_R = \frac{\partial \tau_{ij}}{\partial x_j} = \frac{\partial}{\partial x_j}\left(\overline{u_i' u_j'}\right) \tag{10}$$

A turbulent flow will, compared to a laminar flow, enhance the above properties, and thus a model for the Reynolds stress could be, as proposed by (Boussinesq, 1877):

$$-\overline{u_i' u_j'} = \upsilon_t \left(\frac{\partial U_i}{\partial x_j} + \frac{\partial U_j}{\partial x_i} \right) \tag{11}$$

where υ_t is the eddy-viscosity, or the turbulent viscosity. It is computed using some turbulent quantities, such as the turbulent kinetic energy and the turbulent length scale:

$$\upsilon_t \approx \sqrt{k} l \tag{12}$$

In the commonly employed two-equation EVMs the turbulent kinetic energy is solved using a transport equation, whereas the turbulent length scale is computed using k and secondary (a length-scale determining) turbulent quantity. There exists EVMs based on the dissipation rate of turbulent kinetic energy, ε, the turbulent time-scale, τ or the specific dissipation, ω. These quantities are solved using a transport equation, similar in construction to that shown in Eq. (9). A comprehensive study of two-equation EVMs could be found in (Bredberg, 2001).

2.4 Turbulent heat transfer models

Compared to the large amount of turbulence models for the flow field there exists only a relatively few heat transfer models. This may be a consequence of that the heat transfer model plays an inferior role compared to the turbulence model in predicting heat transfer data (private communication, Raisee, 1998). The coupled nature of the temperature and flow field, and thus the difficulties of accurately measure the heat transfer is however more to blame for the sparse work which has been done on heat transfer models. The appearance of DNS (e.g. Kawamura et. al., 1999) have however made it possible to construct new and more elaborated models, with improved predictability.

The simplest model is the SGDH (Simple Gradient Diffusion Hypothesis) which is based on similarities to the molecular heat transfer:

$$-\overline{u_i' t'} = \frac{\upsilon_t}{Pr_t} \frac{\partial T}{\partial x_i} \tag{13}$$

with Pr_t is the turbulent Prandtl number with a value 0,9 of for air. Kays (Kays, 1994) made a comprehensive review of alternatives to the constant Pr_t. A heat transfer model suitable when a RSM is employed for the flow field is the GGDH (Generalized Gradient Diffusion Hypothesis) which is an adaptation of the Daly-Harlow diffusion model (Daly & Harlow, 1972). The model can incorporate un-alignment effects in the relations for the heat flux vector and the temperature gradient:

$$-\overline{u_i' t'} = C_\theta \overline{u_i' u_j'} \frac{k}{\varepsilon} \frac{\partial T}{\partial x_i} \tag{14}$$

The model however relays on similarities (an extended Reynolds analogy) to the flow-field for any transport effects in the heat flux vector as the GGDH is still a local model. A more fundamental heat transfer model similar to RSM has been developed by Launder et. al., which in a matured form can be found in (Launder, 1989).

2.5 Some numerical consideration of CFD

In the dominating majority of CFD-codes the solution method used for the governing equations, is the Finite Volume Method (FVM). Using this method the particular computational domain is divided into a number of control volumes. The differential versions of Navier-Stokes equations are discretized onto the computational mesh and numerically integrated over the control volumes and then solved until a convergence criteria is reached.

For the computations presented in the next section, the academic CFD-code CALC-BFC (Davidson & Farhanieh, 1995) is used. In the following section the commercial CFD-code ANSYS/Fluent is used (ANSYS, 2001). In either there is a selection of discretizing schemes, where hybrid (Spalding, 1972), central, van Leer (van Leer, 1974) and QUICK (Leonard, 1979) are examples of common used algorithms for pressure-based Navier-Stokes solvers (PBNS). The governing equation for a specific variable are after discretization expressed as:

$$a_p \phi_p = \sum_{nb} a_{nb} \phi_{nb} + S \tag{15}$$

where a_i are the coefficients from the convective and diffusive terms. Index p represents the nodal point and nb the contribution from the neighbouring nodes. Source terms in the governing equations are included in S. For a PBNS this equation system is solved iteratively using a Tri-Diagonal Matrix Algorithm (TDMA).

For incompressible flows the pressure needs to be carefully treated as the equation of state, $P=\rho RT$, is not suitable to use. In both CALC-BFC and ANSYS/Fluent the SIMPLE algorithms are used to deal with the velocity-pressure coupling (Patankar & Spalding, 1970) and (van Doormal & Raithby, 1984).

CALC-BFC uses Boundary-Fitted-Coordinates (BFC), with the nodes and grid points located in a non-staggered (ie. co-located) configuration. This procedure can induce a so-called checker-board solution, due to the velocity-pressure coupling, which is alleviated through the Rhie-Chow (Rhie & Chow, 1983) interpolation scheme.

2.6 Mesh dependencies and discretization schemes

The progress of computer power, which enables increasingly fine mesh to be employed, along with the development of highly accurate discretizing schemes, has reduced the numerical errors. The result of this have made CFD-workers believe that the results from their CFD-codes are purely an effect of the chosen flow models (turbulence models), boundary conditions etc. This is to a certain degree true, however in special cases and for sensitive quantities there is still an influence on the result from numerical approximations made in the CFD-codes and from mesh refinement. To visualize this, two different cases are selected: I) a backward-facing step (BFS) case and II) the heat transfer from a rib-roughened channel. The two cases were simulated using CALC-BFC with both the hybrid and the van Leer discretizing schemes and with different levels of mesh refinement.

Backward facing step (BFS)

The BFS-case is the one studied by Gartling (Gartling, 1990). The Reynolds number is low enough to enable a laminar simulation to be performed. The demands on the discretizing scheme increases as a result, as any numerical (artificial) diffusion will be much more pronounced if it is not clouded by the turbulent diffusion. The geometrical condition is shown in Fig. 2. The expansion rate, i.e. the step-height to channel-height ratio, for this case

is h/H=2. Two different meshes were used in the computations: a 100 x 90 mesh and a 200 x 180 mesh (stream-wise by wall-normal). The inlet was specified as a parabolic profile in U, as in the benchmark (Gartling, 1990). The walls are well resolved on both meshes, with four and six nodes located within $y^+=1$ for the 100 x 90 and 200 x 180 mesh, respectively. In the region of interest the meshes are un-stretched in the stream-wise direction, and only gently stretched in the wall-normal direction, with a maximum ratio, located at the walls of 4% and 1%. The discretizing schemes are here only compared for the predicted cross-stream (V) velocity profiles at x/h=7. This station is located immediately downstream the re-attachment point, at xr/h=6,1 (benchmark data).

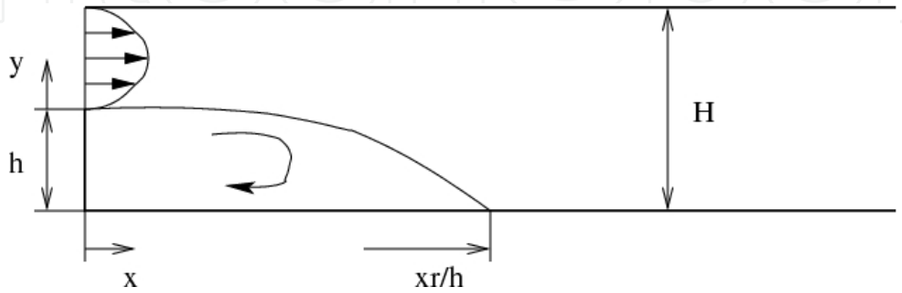


Fig. 2. Geometry of Gartling BFS (Gartling, 1990)

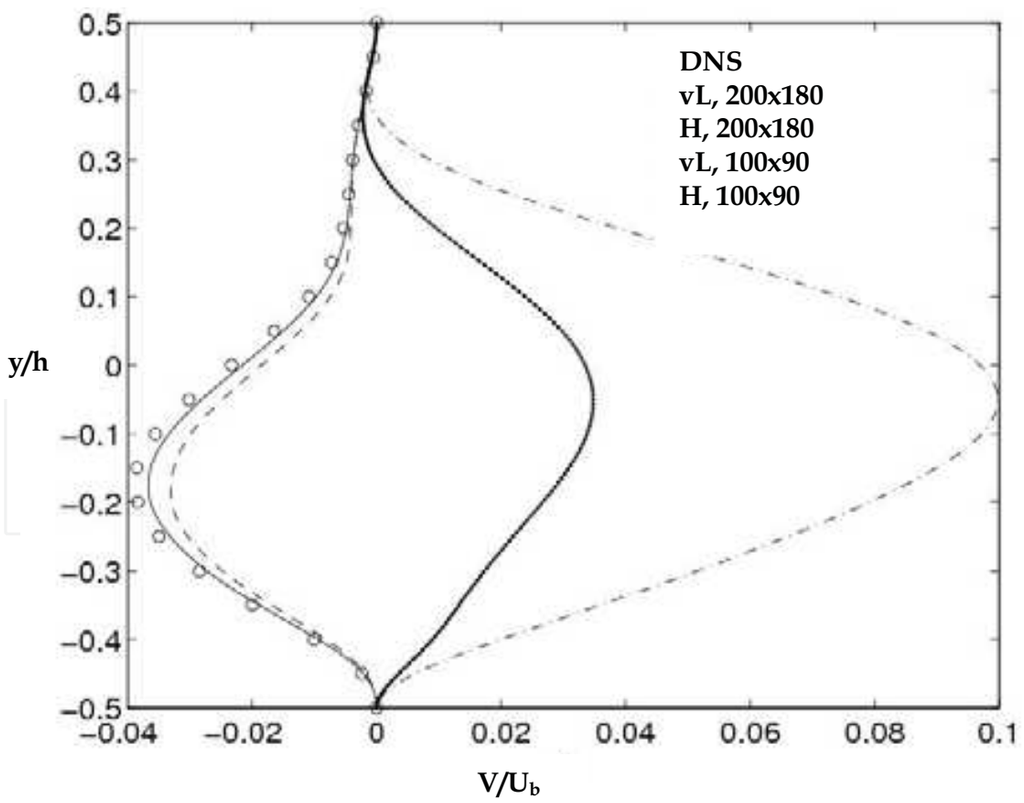


Fig. 3. Vertical velocity at x/h=7, Gartling BFS. Prediction using Hybrid (H) and van Leer (vL) discretization schemes

It is shown in Fig. 3 that the hybrid scheme is extremely sensitive to the used mesh, while the van Leer scheme predicts nearly identical profiles for both meshes, and also in close agreement with the DNS data.

Rib-roughened channel

The rib-roughened channel is the one studied experimentally by Rau et. al. (Rau et. al., 1998) The Reynolds number based on the bulk velocity is Re_H=30.000. The ribs are square with a rib-size of e/H=0.1, and located along the bottom (south) wall with a pitch of P/e=9, see Fig. 4. A constant heat flux boundary condition was applied at the bottom wall, with the rib insulated. The measured and the predicted Nusselt numbers are normalized with the Dittus-Boelter equation (Dittus & Boelter, 1930), as introduced by McAdams (McAdams, 1942):

$$Nu_{\infty} = 0.023\mathrm{Re}^{0.8}\mathrm{Pr}^{0.4} \tag{16}$$

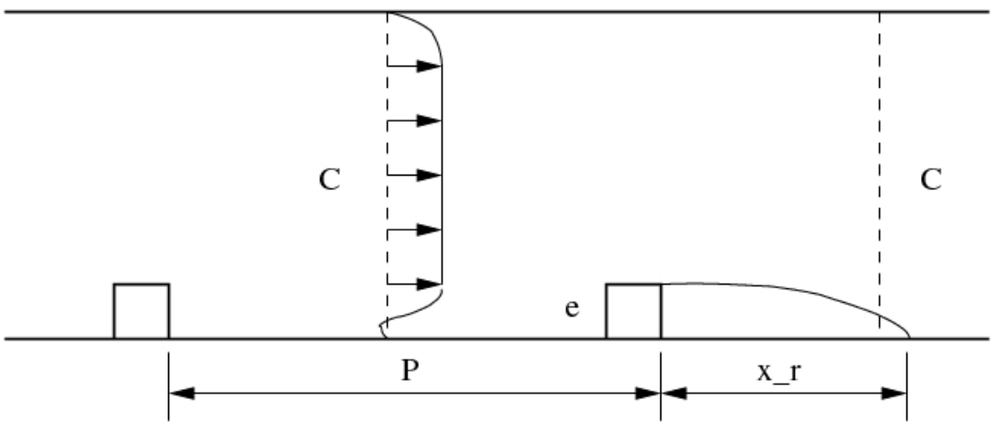


Fig. 4. Geometry, Rib-roughened channel (Rau et. al., 1998)

The computations were made using cyclic boundary conditions (C for cyclic in Fig. 4) at the stream-wise boundaries. Four different meshes were used: one with 200 x 240 nodes, two with 100 x 120 nodes and one with 50 x 60 nodes (stream-wise x wall normal). For the coarsest mesh the first interior computational node was located beyond y^+=1, although within the viscous sub-layer. It was thus of importance to use a turbulence model which is insensitive to the location of the first node. Using the conclusions from Bredberg (Bredberg, 2001), the AKN k-ε turbulence model (Abe et. al., 1994) was selected.
The meshes with some predicted data are summarized in the table below:

Mesh	200x240	100x120*	100x120	50x60
y_1/H	0,00006	0,00012	0,0005	0,002
y_1^+(max)	0,09	0,2	0,7	2,8
stretch	14%	30%	15%	12%
Nu (H)	n/a	190	192	188
Nu (vL)	186	190	191	192

Table 1. Mesh dependency on heat transfer, Nusselt number. Hybrid (H) and van Leer (vL) schemes

The first node distance from the wall is expressed both as y_1/H and normalized with local friction velocity $y_1^+(max)$. The stretch is the growth in size of two successive cells, which should be less than 20% to ensure that the predictions are not corrupted by negligence of higher order terms in the estimation of gradients.

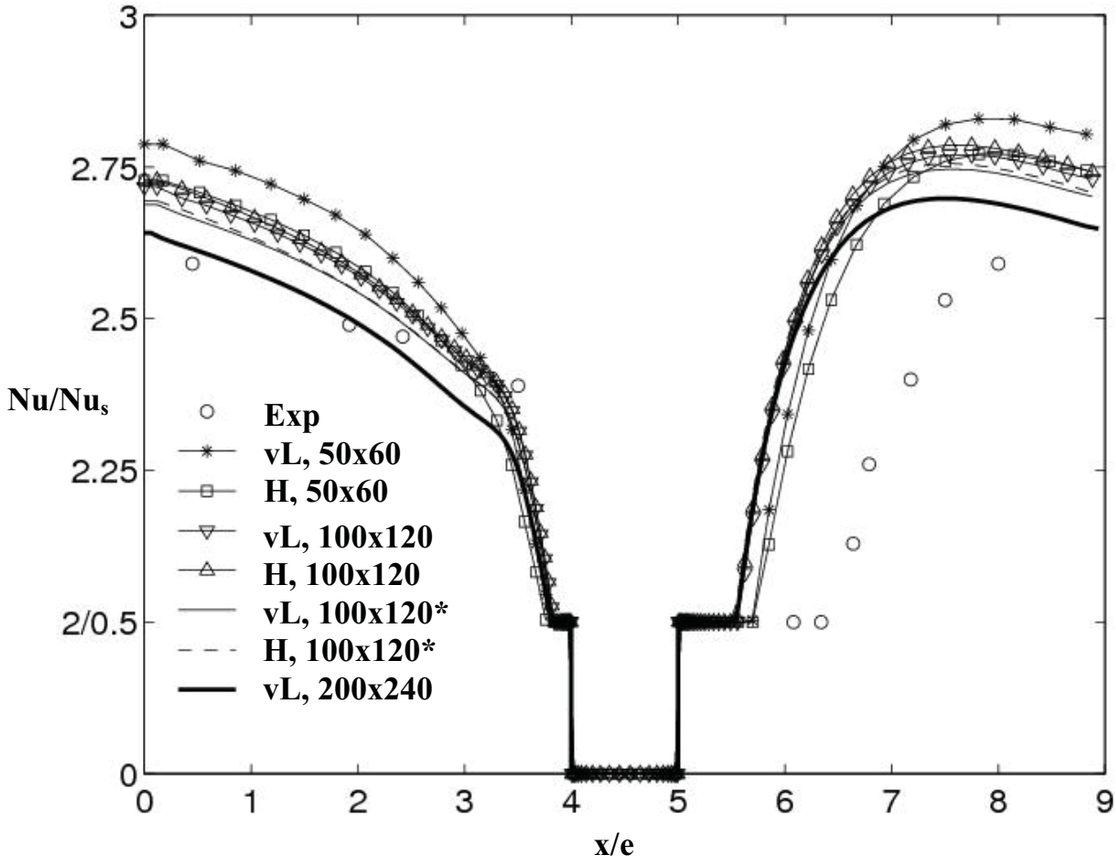


Fig. 5. Normalized Nusselt number for rib-roughened channel (Rau et. al., 1998). Predictions using Hybrid (H) and van Leer (vL) discretizing schemes. Observe the non-uniform y-axis

Fig. 5 gives the predicted variation of the normalized Nusselt number along the south, ribbed, wall. The insulated rib is located at $4<x/e<5$. To more clearly show the difference the graphs are cut for $Nu/Nu_s<2$, which yield a visual impression that there are substantial difference between the predicted results. The maximum deviation is however a mere 5%, which is less than the deviation between two turbulence models as will be shown in the following section. Thus it can be concluded, that for a reasonable re-fined mesh the choice of numerical schemes are irrelevant for heat transfer predictions.

3. Numerical simulations of fundamental flows

A number of two-equations EVMs have been used to compute three different flows: fully developed channel flow, backward-facing-step (BFS) flow and rib-roughened channel flow. The models are: YS, Yang-Shih (Yang & Shih, 1993); AKN, Abe-Kondoh-Nagano (Abe et. al.,

1994); JL, Jones-Launder (Jones & Launder, 1972); C, Chien (Chien, 1982); LSY, Launder-Sharma-Yap (Launder & Sharma, 1974) and (Yap, 1987); WHR, Wilcox-high-Reynolds (Wilcox, 1988) and WLR, Wilcox-Low-Reynolds (Wilcox, 1993). The computations were made using the incompressible finite-volume method code CALC-BFC, (Davidson & Farhanieh, 1995), explained in section 2.5. For all cases only two-dimensional computations were made, to reduce computational costs. The test-cases have been chosen so that the difference between the predicted centreline values for a 3D mesh will be negligible as compared to the used 2D mesh.

3.1 Fully developed channel/pipe flow

The case is a 1D-flow, with a variation only in the wall normal direction. Due to its simplicity this was one of the first cases computed using DNS, and has since then become a standard case for turbulence model comparison. As DNS gives such a wealth of information most designers use these data-bases to improve their models. Thus it is not surprising that the accuracy of post-DNS models (from 1990 and later) are significantly higher than those prior to DNS. The DNS used as a comparison here are the data from Moser et. al. (Moser et. al., 1999), with a Reynolds number based on the channel half width and friction velocity of Re_τ=395.

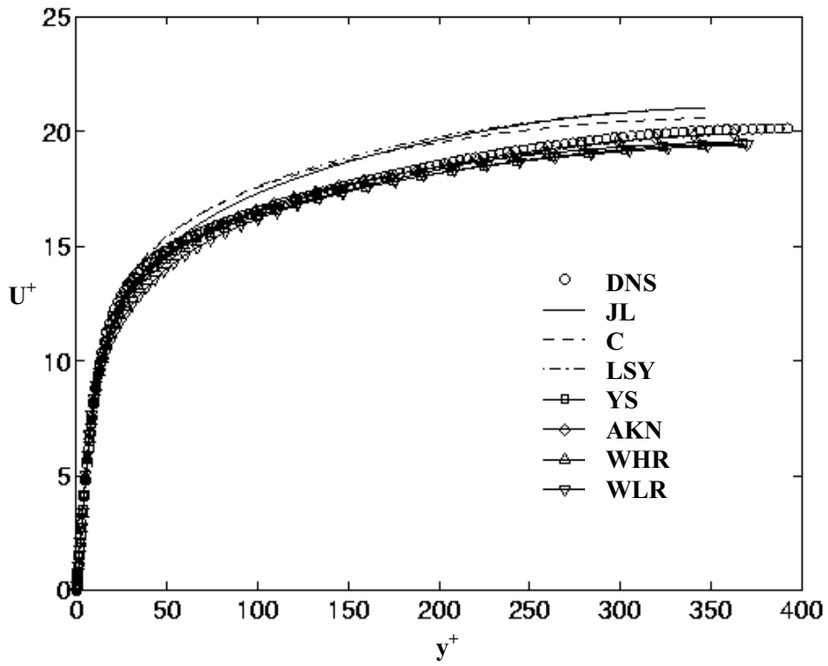


Fig. 6. $U^+=U/U_\tau$ vs. y^+. DNS-data, Moser et. al. (Moser et. al., 1999)

The normalized friction velocity is listed in table 1 along with the predicted Nusselt number using a constant Prandtl number model. The Nusselt number is not available for the DNS-data and instead the Dittus-Boelter equation is used, see Eq. (16). All models predict the friction velocity fairly accurate. The largest deviation for the Nusselt number is given by the JL-model which under-predicts the value by 18%. Note that all turbulence models under-predict the Nusselt number, with the WLR-model yielding a correct value within 2%.

Model	YS	AKN	JL	C	LSY	WHR	WLR
U^*_τ	58,1	57,3	54,8	55,0	54,3	57,5	58,5
Nu	40,1	38,9	33,9	35,6	34,9	38,2	40,4

Table 2. Friction velocity and Nusselt number. DNS, Re_τ=395: U^*_τ = 1000 x U_τ/U_b =56,9 and Nu_{DB}=41,1

The predicted $U^+=U/U_\tau$ profiles are compared in Fig. 6. The difference between the models is only minor, however some models slightly under-predict the friction velocity with a resulting over-prediction of U^+. Progressing to the turbulent kinetic energy, $k^+=k/U^2_\tau$ the profiles are compared in semi-log plots, Fig. 7. The spread between the turbulence models is significantly larger for this quantity as compared to the velocity profiles. Generally the predictions improve the newer the model is. To quantify the models, the predicted maxima are shown in tables 3. Only the JL, LSY and WHR-models give k^+ values that deviate significantly from DNS data. The WLR-model improves the result substantially compared with the WHR, using the added damping functions. However as noticed later, an improvement in the predicted turbulent kinetic energy don't automatically improve results for other quantities.

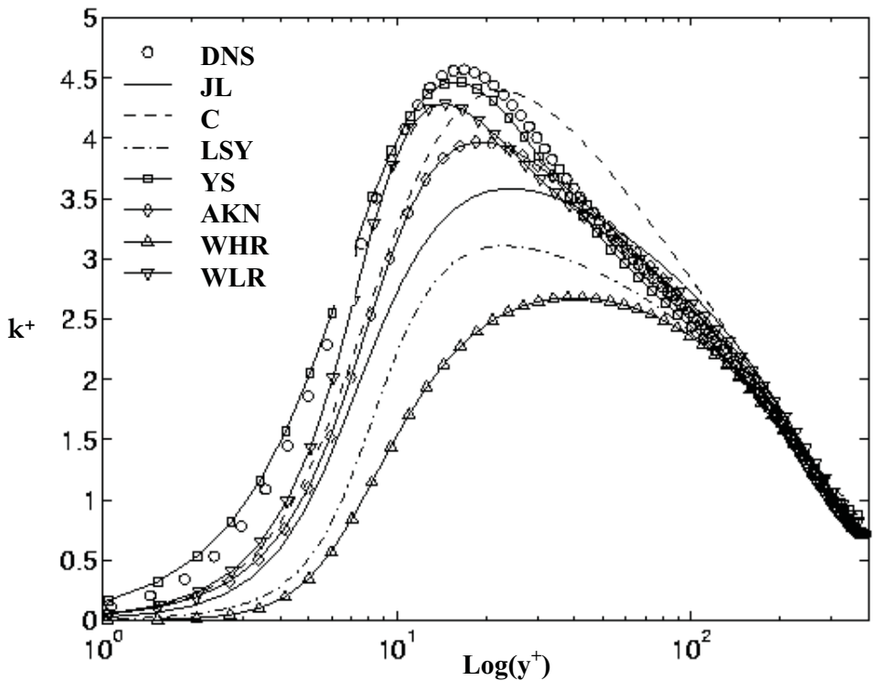


Fig. 7. $k^+=k/U^2_\tau$ vs. y^+. DNS-data, Moser et. al. (Moser et. al., 1999)

Model	YS	AKN	JL	C	LSY	WHR	WLR
k^+	4,47	3,97	3,58	4,39	3,11	2,68	4,29
ε^+	0,29	0,18	0,19	0,21	0,18	0,22	0,13

Table 3. Maximum value of k^+ and ε^+. DNS, Re_τ=395: k^+=4,57 and ε^+=0,22

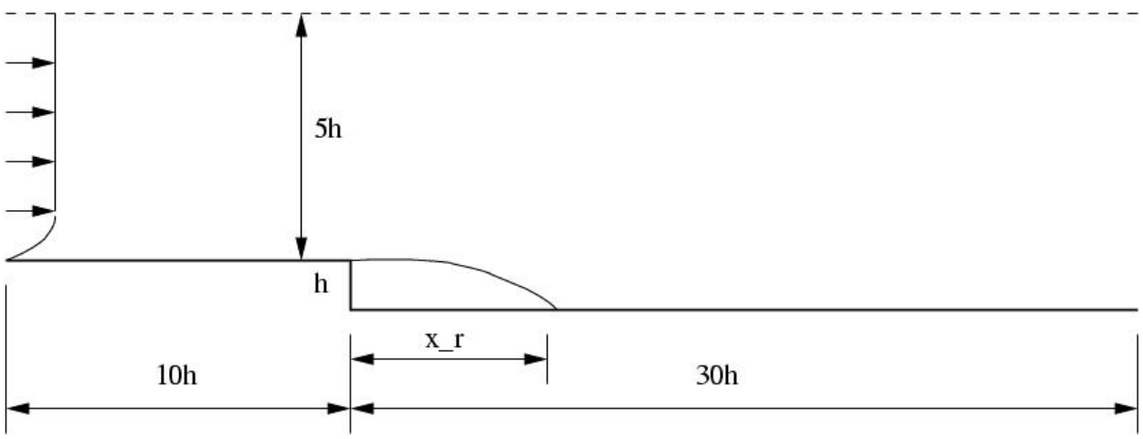


Fig. 8. Geometrical conditions, not to scale, BFS-case (Le et. al., 1997)

3.2 Backward-facing-step flow

In the backward-facing step case, the flow undergoes separation, re-circulation and re-attachment followed by a re-developing boundary layer. In addition, this flow involves a shear-layer mixing process, as well as an adverse pressure, thus the backward-facing step (BFS) is an attractive flow for comparing turbulence models. The case used here is the one that has been studied using DNS by Le et. al. (Le et. al., 1997) see Fig. 8. This case has a relatively low Reynolds number, Re_h=5.100, based on the step-height, h. In the present computation the inflow condition was specified using DNS data at x/h=-10. Neumann condition was applied for all variables at the outlet located at x/h=30. No-slip condition was used on the walls. The overall calculation domain ranges from x/h=-10 to x/h=30, with the step located at x/h=0. The channel height is 5h in the inlet section and 6h after the step, yielding an expansion ratio of 1,2.

The inlet condition in the BFS-case is crucial for a critical evaluation and comparison. The DNS data of Spalart (Spalart, 1988) for the velocity profile and the k-profile, are directly applied at the inlet. The inflow ε or ω was specified in such a way that the model prediction matches the DNS data at x/h=-3.

The skin friction coefficient, defined as $C_f=2\tau_w/(\rho U^2_\infty)$, is shown in Fig 9. The predicted friction coefficient varies from very good (LSY) to rather poor (JL and C). Although hardly discernible, the Chien-model reproduces a highly questionable C_f profile around the re-attachment point. The y^+-based damping functions is the main reason for this spurious behaviour, which also yields erroneous heat transfer in the rib-roughened case.

Model	YS	AKN	JL	C	LSY	WHR	WLR
x_r/h	4,62	5,65	6,17	5,86	6,83	7,46	7,96
$C_{f,max}$	3,68	3,35	4,04	4,05	3,13	2,56	2,30

Table 4. Re-attachment point and maximum friction coefficient. DNS: x_r/h=6,28, 1000 x $C_{f,max}$=3,04

One of the commonly used quantities to justify the accuracy of a turbulence model in a BFS-case is the re-attachment length of the main separation. Table 4 gives the re-attachment length, x_r, using the different models in comparison with DNS data, x_r/h=6,28. The model which yielded the most favourable values for ε^+ at the wall in the channel flow case, YS

completely fail to capture the re-attachment point in this case, by as much as 26%. The Wilcox k-ω models (WHR and WLR) don't give very accurate predictions either, with an overestimation of the re-attachment point of 19% and 27% respectively. Notable is that the improved WLR-model gives worse result.

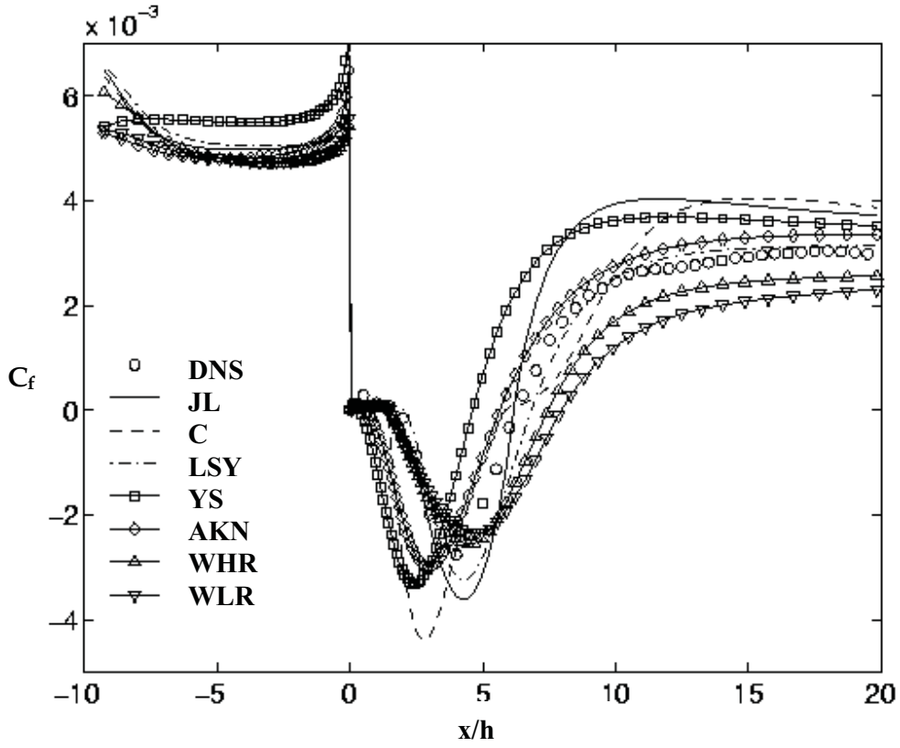


Fig. 9. C_f along lower wall. DNS-data, Le et. al. (Le et. al., 1997)

3.3 Rib-roughened channel flow

The heat transfer performance of the different models is evaluated in the rib-roughened case of Rau et. al. (Rau et. al., 1998) as used in the above mesh sensitivity study, see section 2.5. The Reynolds number, based on the mean velocity and the channel height is Re_H=30.000. The height-to-channel hydraulic diameter, e/H, is 0,1, and the pitch-to-rib-height ratio, P/e=9, see Fig. 4. The experiment provides both flow field and heat transfer measurements, however here only the centre-line Nusselt number is used in the comparison. The measured Nusselt numbers were normalized with the Dittus-Boelter equation see Eq. (16). The uncertainty in the resulting enhancement factor, Nu/Nu_∞ was estimated to be 5% for the experiment.

The computations were made using periodic boundary condition at the stream-wise boundaries, which was verified in the experiment to prevail in the test section. This reduces the uncertainty in the result due to the inlet boundary condition. No-slip condition and constant heat flux were applied at the walls. The rib was, as in the experiment, insulated.

Fig. 10 compare the Nusselt numbers predicted from the different turbulence models.

The AKN model give accurate predicted Nusselt number (+6%) although it yields too high values downstream the rib. The worst results are predicted with the JL and C-models,

especially the C-model, with a large over-prediction of the Nusselt number. The Wilcox models (WHR, WLR) under-predict the Nusselt number by a fair margin. The effect of the Yap-correction is apparent, with the LSY-model predicts less than half the Nusselt number as compared with the JL-model. The former is also in better agreement with the experimental data.

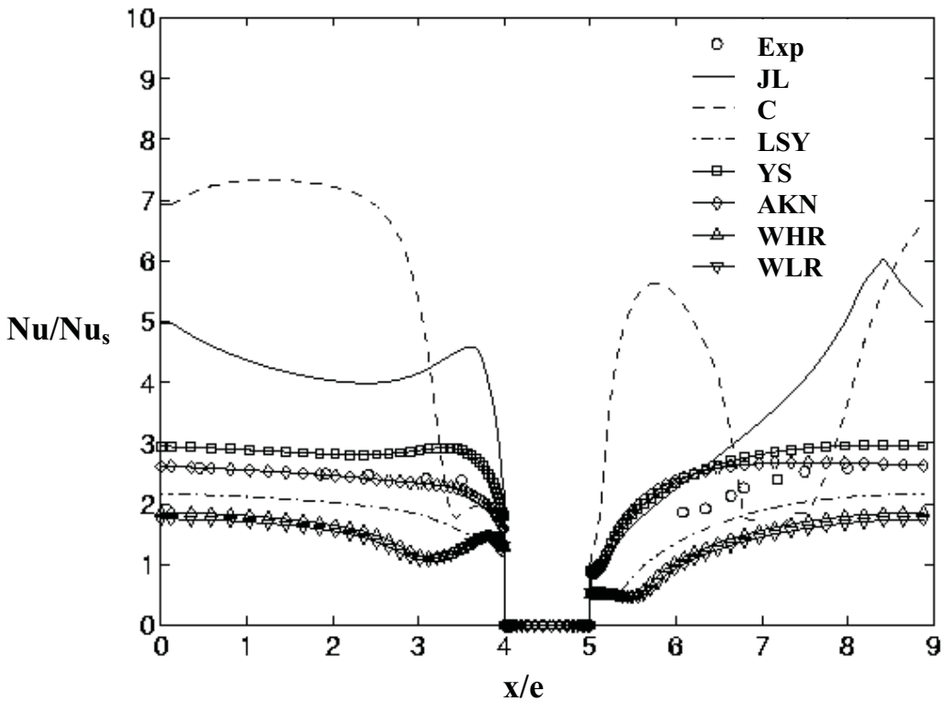


Fig. 10. Nu along lower wall. Experiment, Rau et. al. (Rau et. al., 1998)

Model	YS	AKN	JL	C	LSY	WHR	WLR
Nu_{max}	227	206	463	546	165	142	133
$\int Nu$	206	185	298	368	137	113	106
%	+18	+6	+71	+111	-21	-35	-39

Table 5. Nusselt number. Experiment: $\int Nu \approx 174$, $Nu_{max}=198$

Table 5 give both the average and the maximum Nusselt number for each model along with the deviation of turbulence models from the experiment is also listed.

It is of interest to compare the predicted Nusselt number for the rib-roughened with the predicted skin friction in the BFS-case. In table 4 the maximum C_f in the re-developing zone, i.e. after the re-attachment point is listed.

Using Reynolds analogy it is reasonable to believe that models which underestimate the maximum friction coefficient will also underestimate the heat transfer coefficient. The JL- and C-models that severely over-predict the heat transfer in the rib-roughened case also give too large skin friction. The models that under-predict Nu (WHR, WLR) also gives low values of skin friction in the backward-facing step case.

4. PWR applied CFD simulations

The three simulation cases presented below were all made at Epsilon UC Väst AB in support of Ringhals AB working with ARTIST (Güntay et. al. 2004). Aerosol Trapping In a Steam Generator (ARTIST) was an international project that investigates the consequences of a tube rupture in steam generators in nuclear power plants. A tube fracture in a steam generator could, in worst case, lead to a spread of nuclear substances to the atmosphere. It is therefore of great importance to investigate how such effects can be minimized, should a rupture take place. The ARTIST project was divided into seven phases, with the aim of each phase to investigate, both numerically and experimentally different parts of the steam generator, as visualized in Fig. 11. Note that the aim of the ARTIST project was to investigate the overall retention of nuclear particles in a steam generator, whereas the simulations presented here are all concerned with the flow distribution in a tube bundle. The system simulated is the state formed after a tube break has occurred when the coolant, on the secondary side, has evaporated and the gas from the primary side flows through the bundle.

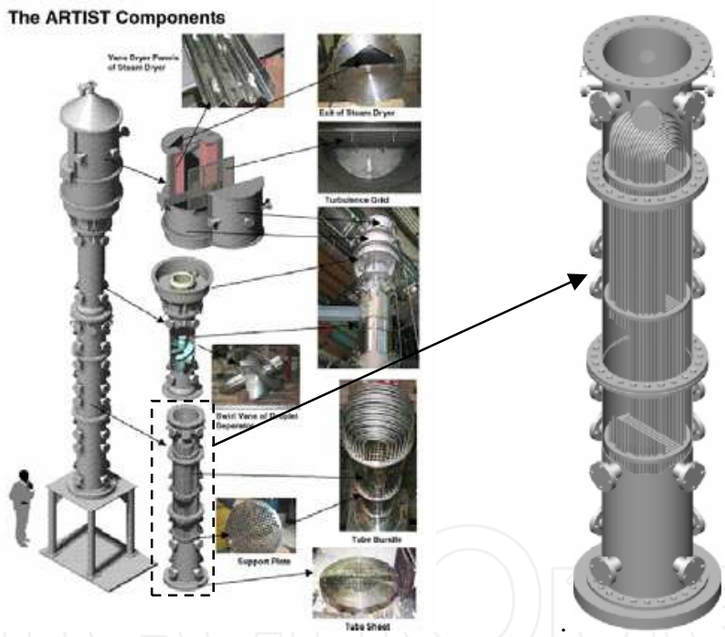


Fig. 11. ARTIST components with steam generator tube bundle enhanced. (Güntay et. al. 2004)

4.1 Flow distribution in a seam generator with a tube failure

The ARTIST scaled-down steam generator, compromises one tube bundle divided into three tube stage, one separator and one dryer as seen in Figure 11. The three stages; break stage, stage 2 and stage 3 are separated by 30mm thick support plates, with a distance between each support plate according to Figure 12 . The diameter of the tube bundle is 573mm. The total number of tubes in a fully occupied tube bundle is 270. The tubes have an inner-diameter of 16,8mm and an outer diameter of 19,08mm. The spacing between them is 27,43mm. In order to achieve a feasible CFD model, the geometry of the tube bundle is only

represented in the break stage, leaving stage 2 and 3 "empty" where porous media is defined. This is done since it is the flow distribution in the break stage that is of interest. The inside of the fractured tube is included in the computational domain.

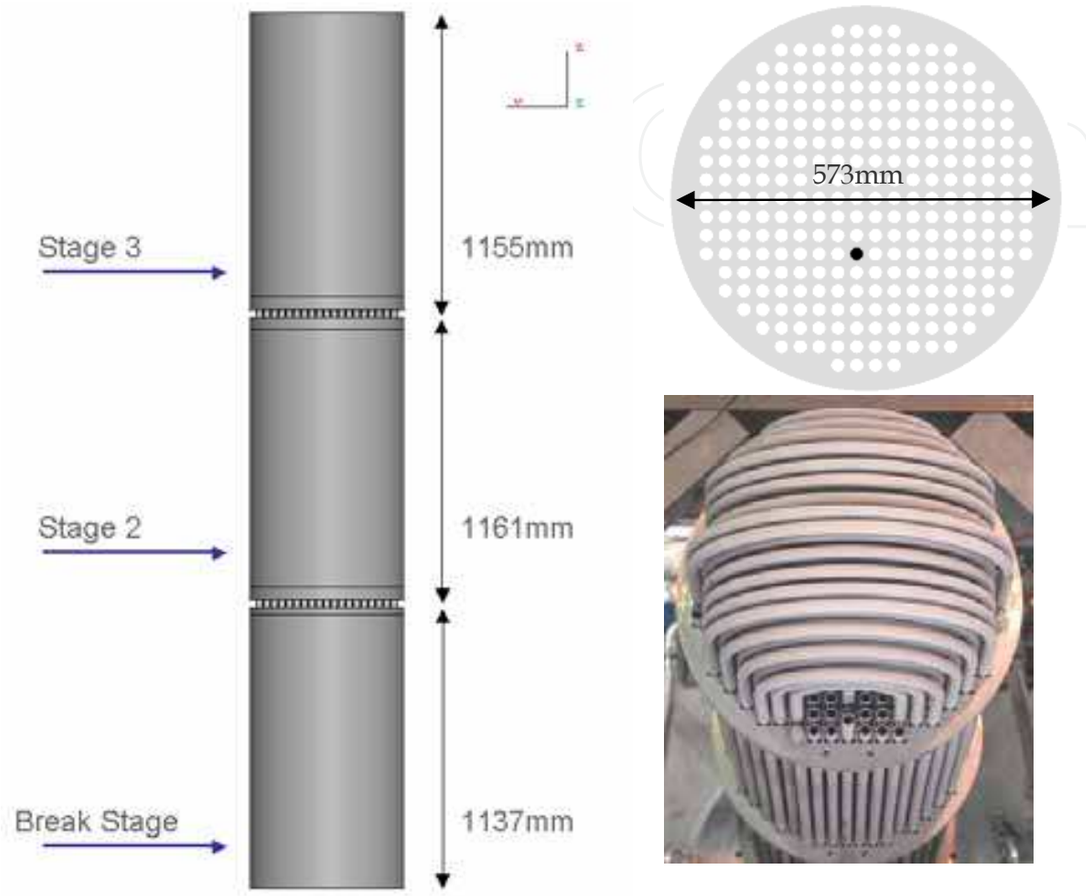


Fig. 12. Main dimension of the ARTIST scale-down steam generator rig. The filled hole in the upper-right figure represent the fractured tube

Figure 13 illustrates the mesh around guillotine break and the four support rods that stabilize the loose ends of the fractured tube. The longitudinal centre of the break is positioned 300mm from the bottom of the break stage. The box inside the break stage is the region close to the break containing the computational mesh shown in figure. This region is resolved with 800.000 computational cells. Total size of the volume mesh in the model is 5,6 million cells where 4,6 million cells are in the break stage and 1 million in the upper stages and support plates.

The CFD code used for solving the flow is ANSYS/Fluent version 6.3. For details of this code, the reader is referred to the users guide and theory guide (ANSYS, 2001). This case is solved with the pressure based RANS implicit iterative and segregated solver assuming steady state and adiabatic conditions. The fluid (nitrogen) is modelled as a compressible ideal gas with constant fluid properties taken at atmospheric condition at a temperature of 298K. The boundary conditions are; pressure at the inlet (4,6atm) and pressure at the outlet (1atm). The walls are modelled using no-slip condition. Stage 2 and 3 are modelled using

porous media for which the pressure loss coefficients are tuned to that of the flow along tubes. Turbulence is modelled using the standard k-ε turbulence model, which is based on the work by Jones and Launder (Jones & Launder, 1972).

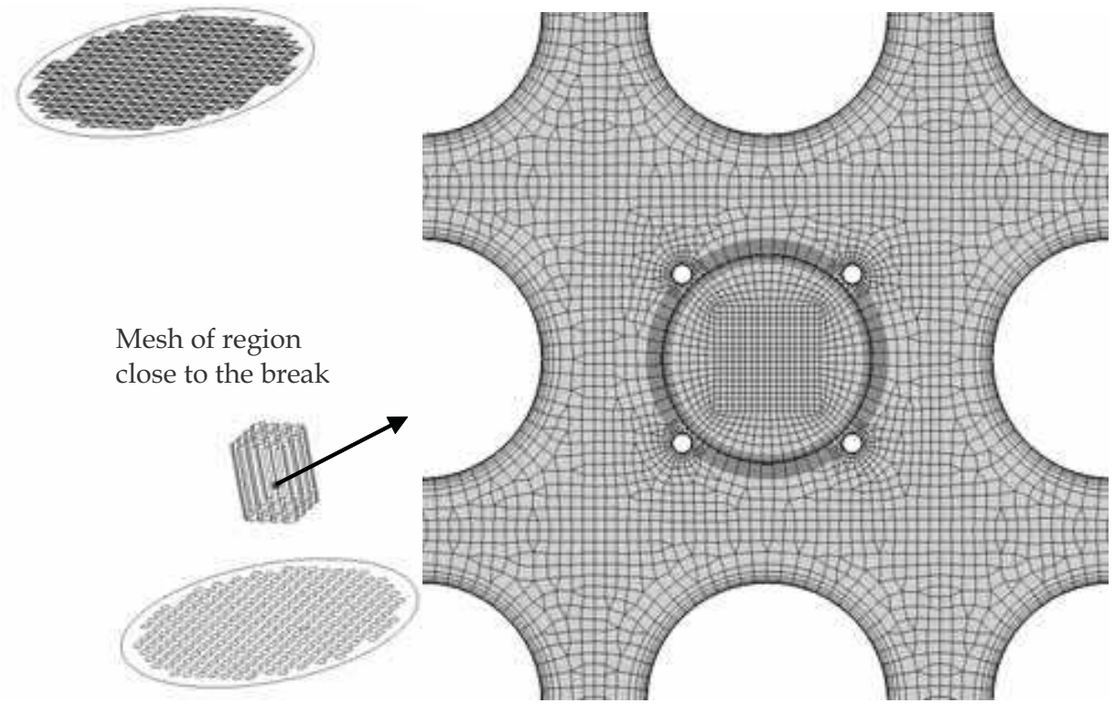


Fig. 13. Computational mesh around the break, including the support rods (voids)

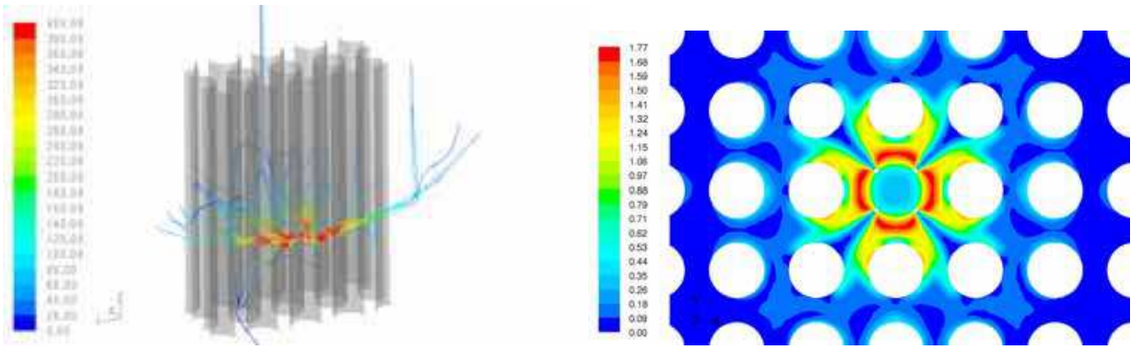


Fig. 14. Flow out from the fractured tube. Left picture; path-lines, coloured with velocity, right picture; contours of Mach-number in a plane through the break

The results focus on the flow distribution in the break stage and the pressure drop throughout the entire domain. The velocities in the upper stages are presented as well but are not physically true since the geometry of the tubes is represented with porous media.
Fig. 14 shows stream lines, coloured by velocity, released from the break and a contour plot of the Mach number at a xy-plane through the break. It is clear that the velocity field is affected of both the tubes and the support rods.

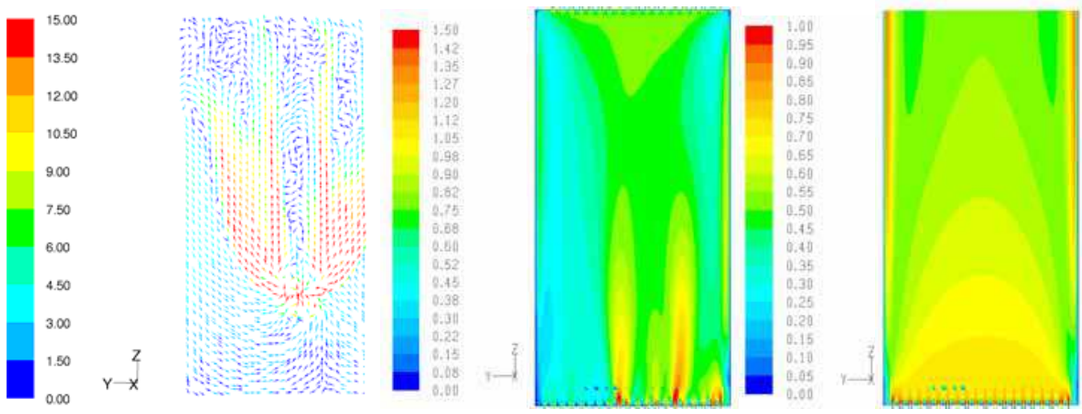


Fig. 15. Velocity variation through the tube bundle. From left to right; velocity vectors in the break stage; velocity contours in stage 2 and velocity contours in stage 3

The vertical velocity through the tube bundle is visualized in Fig. 15. Around the break there is a strong recirculation, illustrated the left in the figure as a vector plot on a xz-plane through the break stage. The computed velocity magnitudes in the upper stages (middle and right pictures in Fig. 15) are, as mentioned earlier, not physically correct since the geometry of the tubs is represented with porous media. The real open cross sectional area in the upper stages is 0,181m², corresponding area in the CFD model is 0,258m². The open area is thus 1,43 times larger in the CFD model. The contour plots below shows that stage 3 has a relatively homogenous velocity distribution. It is however expected that a homogenous distribution develops faster through a porous zone than through real bundle geometry.

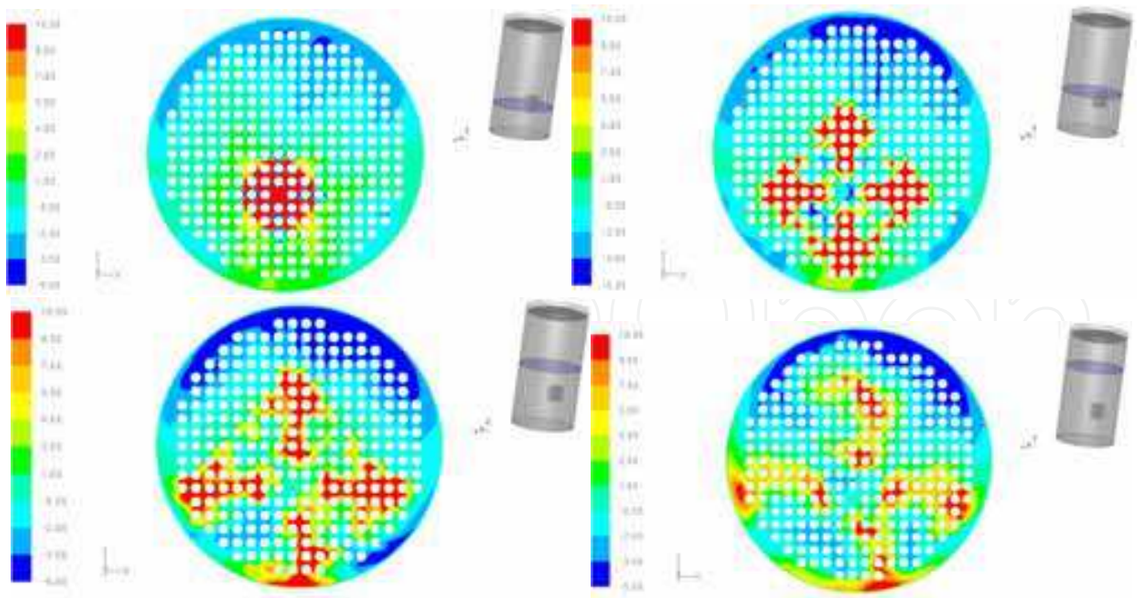


Fig. 16. Vertical velocity at selected horizontal planes. Upper-left: at break position, upper-right: 0,1m above break, lower-left: 0,3m above break and lower-right: 0,5m above break

The flow distribution in the break stage is here visualized with contour plots of vertical velocity (z-velocity) at 4 different planes, see Fig. 16. A sketch of the current plane position is

added beside each contour plot to illustrate where in the break stage the plots are generated. The plots above demonstrate how the flow from the guillotine break develops to four dominant flow streams upwards in the break stage. The region in the tube bundle where most of the recirculation, negative z-velocity, occurs is also visible in the plots. This "negative z-velocity flow" is concentrated to the zone most distant to the break, hence in the upper part of each of the plots above.

The most significant pressure drop occurs when the gas expands out from the broken tube but the pressure drop due to friction inside the tube, before the break, is also considerable.

The table below lists the pressure losses throughout the whole tube bundle. It is clear that the pressure losses in the upper stages and in the support plates are insignificant compared to the losses in the break stage.

Section of the tube bundle	Pressure drop, total pressure
Break tube	20.5kPa
Break stage	338.2kPa
Support plate 1	17.8Pa
Stage 2	1.8Pa
Support plate 2	6.2Pa
Stage 3	1.7Pa

Table 6. Pressure drop in total pressure

4.2 Flow simulation of a Beznau steam generator

In the ARTIST project the Beznau power plant (365MW, Westinghouse design) was chosen as the basis for investigation. Each steam generator at Beznau consists of close to 6500 tubes in a cylindrical shaped enclosure, while the test rig, consists of 274 tubes, in an octagonal box. This rig shares the same tube dimensions with the above steam generator rig, i.e. an outer diameter of 19mm and an inner diameter of 16,8mm. The guillotine break (horizontal cut) is positioned at roughly 1/4 of the height in a centrally located tube. The purpose of this rig is to enable velocity measurement using LDA, which was not possible in the above steam generator rig. The choice of an octagonal Plexiglas rig improved visibility and access, however reduced the maximum pressure. There are thus three different simulation using two different geometries:

- The Beznau steam generator with 6500 tubes, with a mass-flow of 650kg/h
- The ARTIST model with 274 tubes, with a mass-flow of 650kg/h
- The ARTIST model with 274 tubes, with a mass-flow of 360kg/h for comparison with LDA measured velocities

The two computational domains are shown in Fig. 18. For both cases a single stage (the break stage) is modelled. The Beznau mesh has 25 million cells, while the ARTIST model consists of 6 million cells.

The simulations were performed with the CFD-code ANSYS/Fluent (ANSYS, 2001), version 6.3.26. Similar to above the pressure based RANS implicit iterative and segregated solver assuming steady state and adiabatic conditions was used. The fluid (nitrogen) is modelled as a compressible ideal gas with constant fluid properties taken at atmospheric condition at a temperature of 298K. Two different turbulence models; k-ε (standard) (Jones & Launder, 1972) and Reynolds Stress Model (with wall reflection enabled) (Launder, 1989), both using enhanced wall treatment (hybrid wall functions). The presented results are converged to at

least 3 orders of magnitudes with second order (upwind-weighted) accurate discretization schemes. Due to numerical instability issues, the turbulence equations for the RSM were solved with first order schemes. Furthermore the flow shows tendencies of unsteadiness away from the break, and consequently a transient simulation was performed to visualize the effects of flow oscillation.

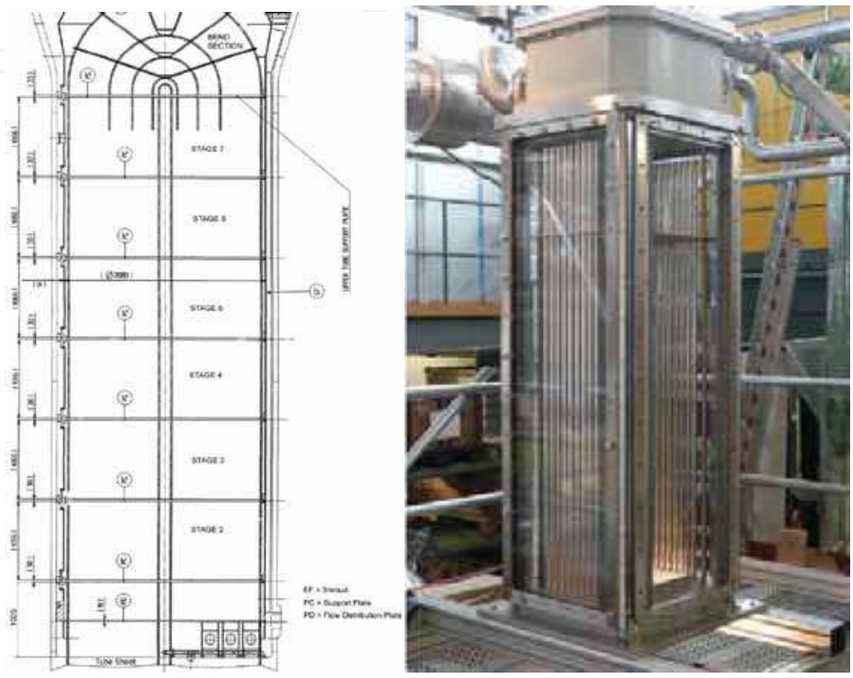


Fig. 17. Schematic drawing of the tube bundle of Beznau steam generator (left) and ARTIST test rig with a octagonal tube bundle for LDA measurements (right)

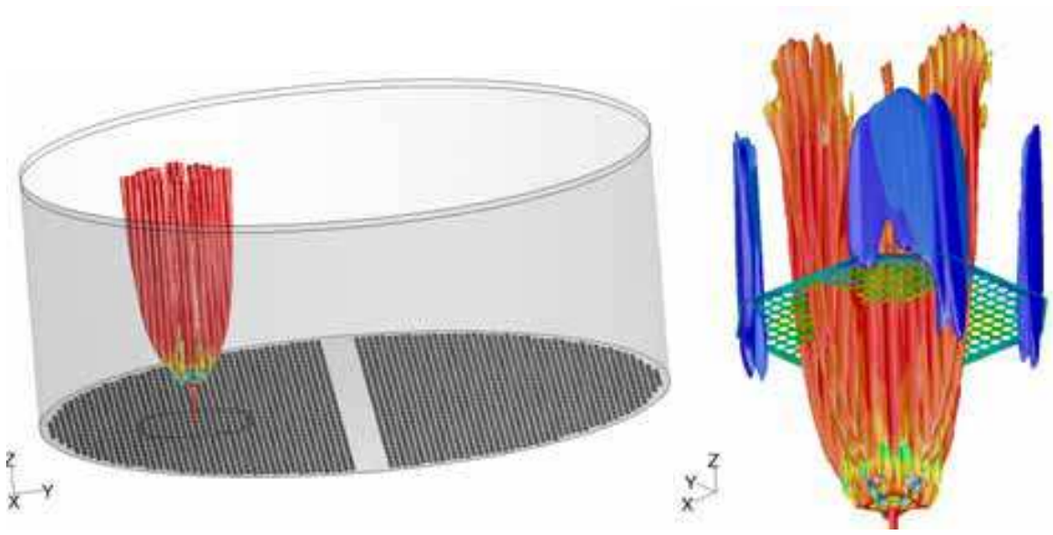


Fig. 18. Apprehension of the significant difference in size. Beznau (left) compared with ARTIST test rig (right)

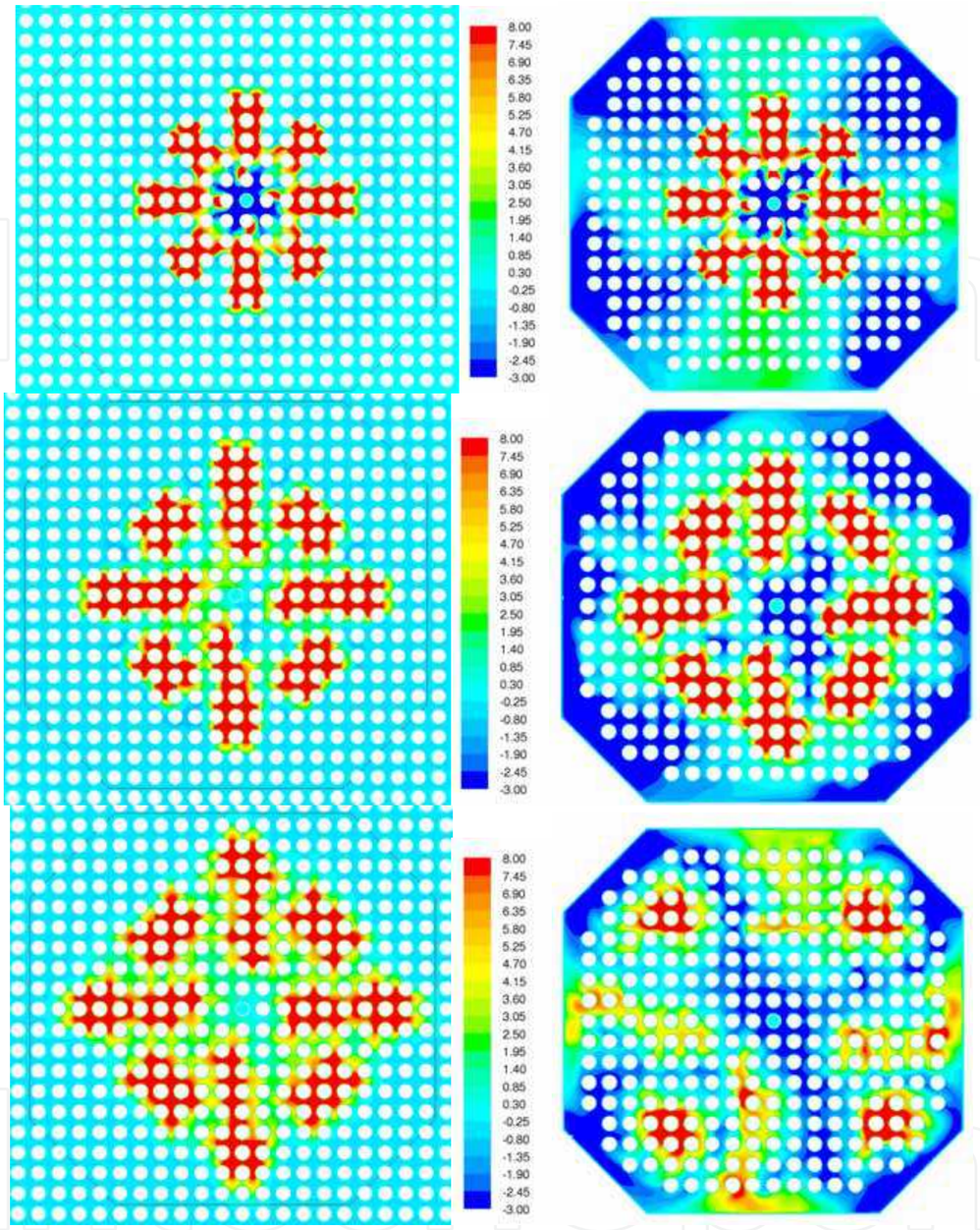


Fig. 19. Contours of vertical velocity for 650kg/h case at horizontal planes above the break. Left: Beznau case (domain cropped), right: ARTIST test rig. Upper row, Δz=100mm, middle row, Δz=350mm z= and lower row Δz=750mm

Figure 19 compares the vertical velocity at selected horizontal planes above the break. The confinement of the test rig gives rise to larger variations, with alternating vertical velocities towards the walls. In contrast, the simulation of the Beznau steam generator shows a very small overall negative velocity, which is a consequence of continuity. The flow field in the vicinity of the break (the central tubes) is unaffected by the boundaries, hence the test rig simulation gives a faithful representation of the flow in this part of the Beznau steam generator.

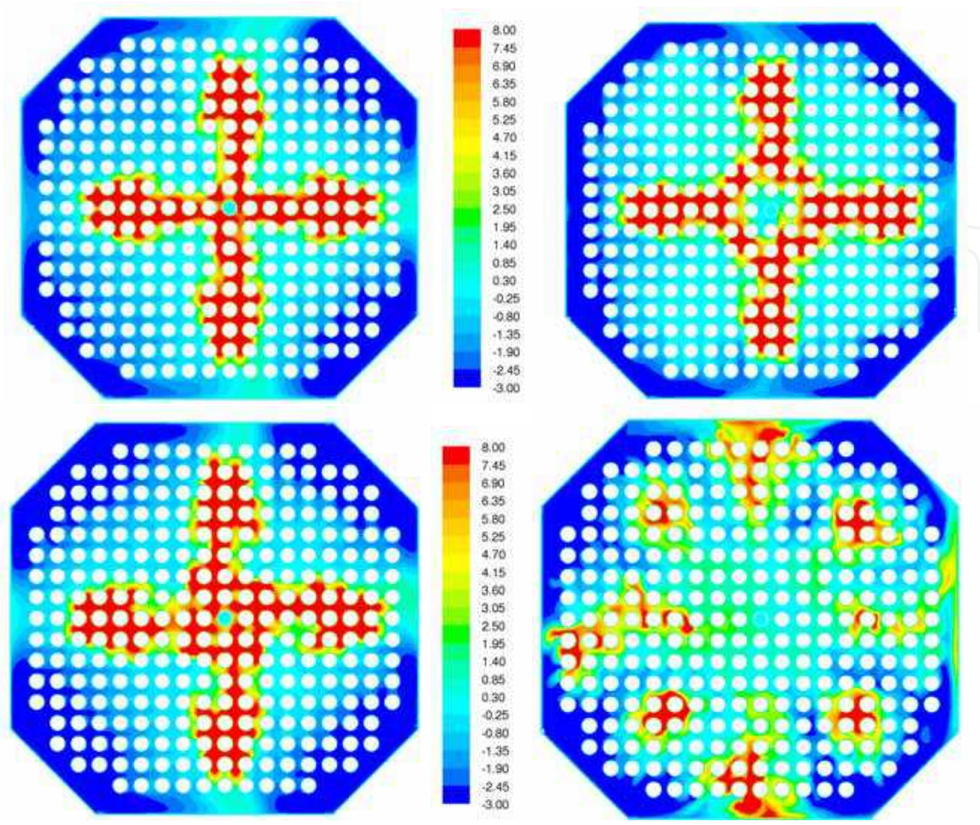


Fig. 20. Vertical velocity at Δz =350mm for 360kg/h case. k-ε 1:st order (upper left), k-ε 2:nd order (upper right), RSM 1:st order (lower left) and RSM 2:nd order (lower right)

The effect of turbulence model and order of discretization scheme can be seen in Fig. 20, where k-ε is compared with the RSM for the test rig domain. Note that the mass flow is different as compared to Fig. 19. It is obvious that the discretization scheme has a more significant importance for the RSM than for the k-ε turbulence model. A comparison between measurements and these turbulence models are presented in Fig. 21.

The measurements were carried out using LDA for a mass flow of 360kg/h. along several lines at two different heights. Sampling was performed to ensure statistical invariance, with around 2000 samples for each measured point. Here comparisons along two lines at 600mm height presents (Δz =350mm. i.e. 350mm above the break). The two lines are shown in Fig. 21, one positioned very close to the break tube (though 350mm above the break), at y=13,7mm, and one closer to the boundaries at y=96mm.

The difference between measured and computed data is clearly notable in Fig. 21, especially for the results based on the k-epsilon turbulence model where the tendency is clearly wrong. Reynolds stress model does a better job, even though the amplitude is not correct. A major reason to the discrepancies between measured and computed data is the rather poor grid resolution in the CFD-model. The total cell count is 6 million cells, but there are still only 6 cell rows between each pair of tubes. This cell distribution combined with highly varying velocity magnitudes, results in y+ values between 0,1 and 256, which may be too demanding on the wall treatment model.

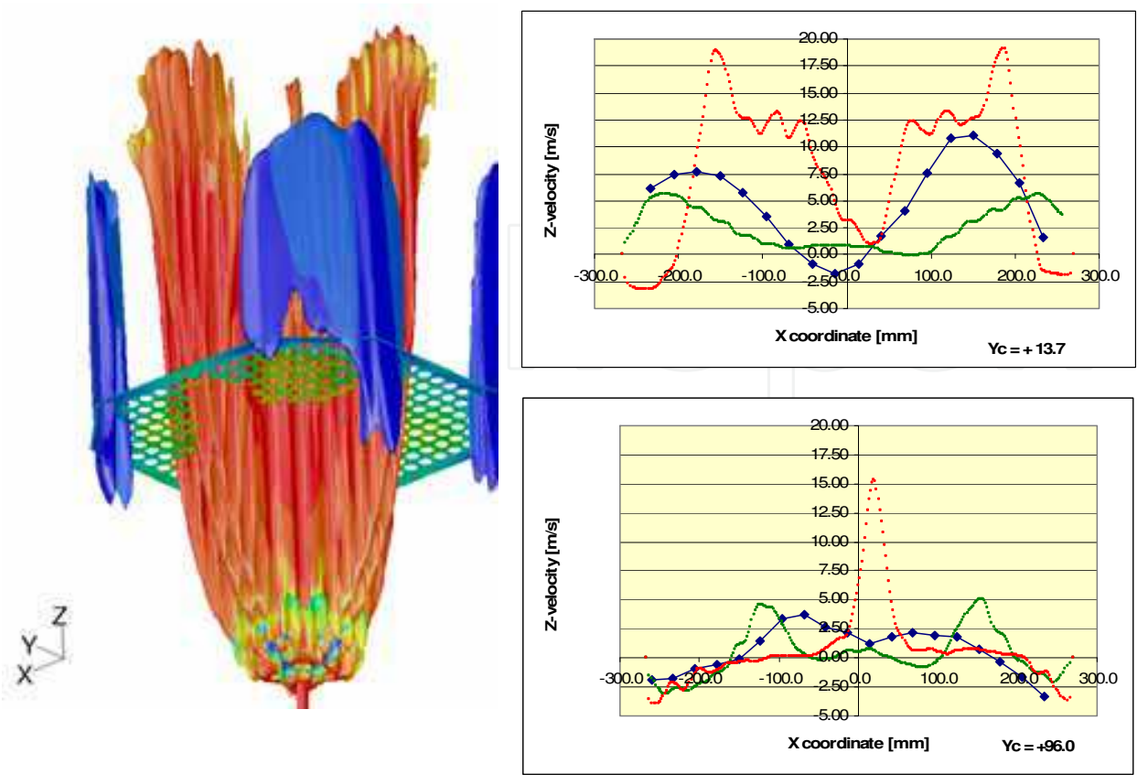


Fig. 21. Right: Z-velocity profile, k-epsilon (red), RSM (green) and measurements (blue). Left: location of measurements

5. References

Abe, K.; Kondoh, T. & Nagano, Y. (1994). A new Turbulence Model for Predicting Fluid Flow and Heat Transfer in Separating and Reattaching Flows - I. Flow Field Calculations, *Int. J. Heat and Mass Transfer*, Vol 37, pp. 139-151

ANSYS/Fluent (2001). *Users guide*, Fluent Inc.

Berg, T.; Bredberg, J. & Dehbi, A. (2008a). Numerical Modeling of Flow in Dry Secondary Side of Steam Generator, *Proceedings of the 2008 International Congress on Advances in Nuclear Power Plants (ICAPP '08)*, ISBN: 0-89448-061-8, Anaheim, June 2008, American Nuclear Society

Berg, T.; Bredberg, J. & Suckow, D. (2008b). CFD Simulation of ARTIST Break Stage and Comparison with Measured Data, *Proceedings of the 2008 International Congress on Advances in Nuclear Power Plants (ICAPP '08)*, ISBN: 0-89448-061-8, Anaheim, June 2008, American Nuclear Society

Boussinesq, T.V. (1877). Mém. pres Acad. Sci.,3rd ed Paris XXIII, pp. 46

Bredberg, J. (1999). *Prediction of flow and heat transfer inside turbine blades using EARSM, k-ε and k-ω turbulence models*, Thesis for the Degree of Licentiate of Engineering, Dept of Thermo and Fluid Dynamics, Chalmers University of Technology, Gothenburg

Bredberg, J. (2001). *On Two-equation Eddy-Viscosity Models*, Internal Report 01/8, Dept of Thermo and Fluid Dynamics, Chalmers University of Technology, Gothenburg

Bredberg, J. (2002). *Turbulence Modelling for Internal Cooling of Gas-Turbine Blades,* Ph.D. Thesis, Dept of Thermo and Fluid Dynamics, Chalmers University of Technology, Gothenburg

Chien, K.Y. (1982). Predictions of Channel and Boundary-Layer Flows with a Low-Reynolds-Number Turbulence Model, *AIAA Journal* ,Vol 20, pp. 33-38

Daly, B.J. & Harlow, F.H. (1970). Transport equation in turbulence, *Physics of Fluids*, Vol 13, pp. 2634-2649

Davidson, L. & Farhanieh, B. (1995). *CALC-BFC*, Internal Report 95/11, Dept of Thermo and Fluid Dynamics, Chalmers University of Technology, Gothenburg,

Dittus, F.W. & Boelter, L.M.K. (1930). Heat transfer in automobile radiators of the tubular type, *Univ. of Calif. Pubs. Eng*., Vol 2, 1930, pp. 443-461

Doormal (van), J.P. & Raithby, G.D. (1984). Enhancement of the SIMPLE Method for Predicting Incompressible Fluid Flows, *Numerical Heat Transfer*, Vol 7, pp. 147-163

Gartling, D.K. (1990). A test problem for outflow boundary condition - flow over a backward-facing step, *Int. J. Numerical Methods in Fluids*, Vol 11, pp. 953-967

Güntay S., Suckow, D., Dehbi, A. & Kapulla, R. (2004).). Artist: Introduction a first results, *Nuclear Engineering and Design*, Vol 232, pp. 109-120

Hinze, J.O. (1975) *Turbulence*, McGraw-Hill Inc.

Jones, W.P. & Launder, B.E. (1972). The prediction of laminarization with a two-equation model of turbulence, *Int. J. Heat and Mass Transfer*, Vol 15, pp. 301-314

Kawamura, H.; Abe, H. & Matsuo, Y. (1999). DNS of Turbulent Heat Transfer in Channel Flow with Respect to Reynolds and Prandtl Number Effects, *Int. J. Heat and Fluid Flow*, Vol 20, pp. 196-207

Kays, W.M. (1994). Turbulent Prandtl number - where are we?, *J. Heat Transfer*, Vol 116, pp. 284-295

Launder, B.E. (1989). Second-Moment Closure: Present… and Future?, *Int. J. Heat and Fluid Flow,* Vol 10, No 4, December 1989, pp. 282-300

Launder, B.E. & Sharma, B.I. (1974). Application of the energy-dissipation model of turbulence to the calculation of flow near a spinning disc, *Letters in Heat and Mass Transfer*, Vol 1, pp. 131-138

Le, H.; Moin, P. & Kim, J. (1997). Direct numerical simulation of turbulent flow over a backward-facing step, *J. Fluid Mechanics*, Vol 330, pp. 349-374

Leer (van), B. (1974). Towards the ultimate conservative difference Monotonicity and conservation combined in a second-order scheme, *J. Computational Physics*, Vol 14, pp. 361-370

Leonard, B.P. (1979). A Stable and Accurate Convective Modelling Procedure based on Quadratic Upstream Interpolation, *Comp. Meth. Appl. Mech. Eng*., Vol 19, pp. 59-

McAdams, W.H. (1942). *Heat Transmission*, McGraw-Hill, New York

Moser, R.D.; Kim, J. & Mansour, N.N. (1999). Direct Numerical Simulation of Turbulent Channel Flow up to Re=590, *Physics of Fluids*, Vol 11, pp. 943-945

Panton, R.L. (1995). *Incompressible flow*, John-Wiley and Sons Inc.

Patankar, S.V. & Spalding, D.B. (1970). *Heat and Mass Transfer in Boundary Layers*, Intertext Books, London

Pope, S.B. (1975). A more general effective-viscosity hypothesis, *J. Fluid Mechanics*, Vol 72, pp. 331-340

Rau, G., Cakan, M., Moeller, D. & Arts, T. (1998). The effect of periodic ribs on the local aerodynamic and heat transfer performance of a straight cooling channel, *J. Turbomachinery*, Vol 120, pp. 368-375

Reynolds, O. (1895). On the Dynamical Theory of Incompressible Viscous Fluids and the Determination of the Criterion, *Ph. Trans. Royal Soc. London, Series A*, Vol 186, pp. 126-

Rhie, C.M. & Chow, W.L. (1983). Numerical Study of the Turbulent Flow Past an Airfoil with Trailing Edge Separation, *AIAA Journal*, Vol 21, pp. 1525-1532

Smagorinsky, J. (1963). General Circulation Experiments with the Primitive Equations I. The Basic Experiment, *Monthly Weather Review*, Vol 91, 1963, pp. 99-165

Spalart, R.P. (1988). Direct Simulation of a turbulent boundary layer up to R_θ=1410, *J. Fluid Mechanics*, Vol 187, pp. 61-98

Spalding, D.B. (1972). A novel finite difference formulation for differential expressions involving both the first and second derivates, *J. Numerical Methods Eng*., Vol 4, pp. 551-559

Wallin, S. & Johansson, A. (2000). An Explicit Algebraic Reynolds Stress Model for Incompressible and Compressible Turbulent Flows, *J. Fluid Mechanics*, Vol 403, pp. 89-132

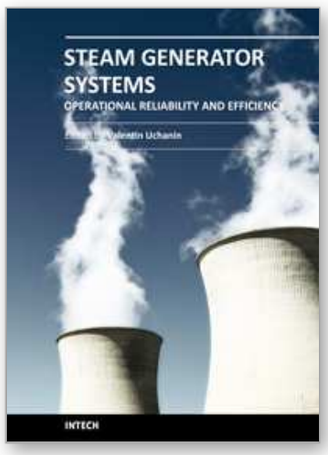
Wilcox, D.C. (1988). Reassessment of the Scale-Determining Equation for Advanced Turbulence Models, *AIAA Journal*, Vol 26, pp. 1299-1310

Wilcox, D.C. (1993). Comparison of Two-Equation Turbulence Models for Boundary Layers with Pressure Gradient, *AIAA Journal*, Vol 31, pp. 1414-1421

Yang, Z. & Shih, T.H. (1993). New Time Scale Based k-ε Model for Near-Wall Turbulence, *AIAA Journal*, Vol 31, pp. 1191-1198

Yap, C.R. (1987). *Turbulent heat and momentum transfer in recirculation and impinging flows*, Ph.D. Thesis Dept. of Mech. Eng., Faculty of Technology, Univ. of Manchester

IntechOpen



Steam Generator Systems: Operational Reliability and Efficiency
Edited by Dr. Valentin Uchanin

ISBN 978-953-307-303-3
Hard cover, 424 pages
Publisher InTech
Published online 16, March, 2011
Published in print edition March, 2011

The book is intended for practical engineers, researchers, students and other people dealing with the reviewed problems. We hope that the presented book will be beneficial to all readers and initiate further inquiry and development with aspiration for better future. The authors from different countries all over the world (Germany, France, Italy, Japan, Slovenia, Indonesia, Belgium, Romania, Lithuania, Russia, Spain, Sweden, Korea and Ukraine) prepared chapters for this book. Such a broad geography indicates a high significance of considered subjects.

How to reference
In order to correctly reference this scholarly work, feel free to copy and paste the following:

Jonas Bredberg (2011). Computation of Flows in Steam Generators, Steam Generator Systems: Operational Reliability and Efficiency, Dr. Valentin Uchanin (Ed.), ISBN: 978-953-307-303-3, InTech, Available from: http://www.intechopen.com/books/steam-generator-systems-operational-reliability-and-efficiency/computation-of-flows-in-steam-generators

INTECH
open science | open minds

InTech Europe
University Campus STeP Ri
Slavka Krautzeka 83/A
51000 Rijeka, Croatia
Phone: +385 (51) 770 447
Fax: +385 (51) 686 166
www.intechopen.com

InTech China
Unit 405, Office Block, Hotel Equatorial Shanghai
No.65, Yan An Road (West), Shanghai, 200040, China
中国上海市延安西路65号上海国际贵都大饭店办公楼405单元
Phone: +86-21-62489820
Fax: +86-21-62489821

© 2011 The Author(s). Licensee IntechOpen. This chapter is distributed under the terms of the Creative Commons Attribution-NonCommercial-ShareAlike-3.0 License, which permits use, distribution and reproduction for non-commercial purposes, provided the original is properly cited and derivative works building on this content are distributed under the same license.

IntechOpen

IntechOpen